Article

Not peer-reviewed version

Characterization of Industrial High-Strength Aluminum Alloys by Laser-Induced Breakdown Spectroscopy, With Special Emphasis on the Detection of Low Contents of Mg, Mn, Cr, Cu, Zn and Sensing of Molecular Diatomic Emission of AlO During Ablation

Svetlana Rytchkova * and Luc Lévesque

Posted Date: 16 February 2024

doi: 10.20944/preprints202402.0890.v1

Keywords: Laser-induced breakdown spectroscopy (LIBS); Aluminum (Al); Magnesium (Mg); Manganese (Mn); Chromium (Cr); Copper (Cu); Zinc (Zn); Aluminum Monoxide (AlO).

Article

Characterization of Industrial High-Strength Aluminum Alloys by Laser-Induced Breakdown Spectroscopy, with Special Emphasis on the Detection of Low Contents of Mg, Mn, Cr, Cu, Zn and Sensing of Molecular Diatomic Emission of AlO during Ablation

Svetlana Rytchkova * and Luc Lévesque

Royal Military College of Canada, Physics and Space Science Department, Kingston, On K7K 7B4, Canada; luc.levesque@rmc-cmr.ca

* Correspondence: svetlana.rytchkova@rmc-cmr.ca

Abstract: The wealth of data obtained during the past 20 years using Laser-Induced Breakdown Spectroscopy (LIBS) indicates that the technique is very promising to detect small chemical contents of alloying elements. The potential of LIBS was looked more seriously during the past two decades or so as more data were obtained on Aluminum and steel to study the phenomena in the condition of local thermodynamic equilibrium and time-delay between a Q-switch laser and an intensified CCD camera. Since the past decade, some data on compounds were also shown to be useful in determining small concentrations of harmful elements. This manuscript is intended to show that the technique of LIBS performance is very promising in fields such as micro-machining, in alloying element analysis, surface cleaning and environmental applications even with lightweight spectrometers having a relatively low resolution, which can potentially be air-borne.

Keywords: Laser-induced breakdown spectroscopy (LIBS); Aluminum (Al); Magnesium (Mg), Manganese (Mn), Chromium (Cr), Copper (Cu), Zinc (Zn), Aluminum Monoxide (AlO).

1. Introduction

The smog in the streets of the Dickensian London in the nineteenth century has evolved to dust emission from toxic industrial waste in the air worldwide, which has affected the ozone layer of the Earth. As a result, the society became more concerned about contamination of soil and in what is absorbed by vegetables consumed in human diets [1]. The world population increased from 1 billion to about 7.8 billion between 1950 and 2020. Therefore, the need for industrial operations became very much more demanding. This demand increased the contamination from the industrial waste that deposit into soil and the need to detect harmful elements were seriously considered in research environment [2,3]. Very precise contaminant detection such as Inductively Coupled Plasma/ Optical Emission Spectroscopy (ICP/OES) and Atomic Absorption Spectroscopy (AAS) were developed and were very successful in detecting small concentrations of harmful elements. Unfortunately, ICP/OES and AAS are very costly, rather bulky and require tedious sample preparation [4]. Various authors looked at the characterization of the plasma gas during LIBS investigations to improve detection of alloying elements in Aluminum [5–7] and to detect Carbon (C) in Carbon thin films [8]. Apart from detection of alloying elements in metals, LIBS was shown to be successful in detecting small contaminants in food during the past 5 to 10 years, such as seafood [9], mango leaf, carrot, potato and meatballs [10]. LIBS were also applied to detect toxic elements such as lead (Pb) in bones from slaughtered animal [11], to detect toxic metal accumulation in hard tissue [12], for characterization of malignant tissue cells [13], in forensic science [14], in archeology [15], for overlaying pigment identification in paintings [16] and in production control in the industry [17]. One of the objectives in

 doi:10.20944/preprints202402.0890.v1

the afore-mentioned applications [14–17] is to detect the constituents of a material such as Al so we may distinguish one type of Al from the other.

This manuscript is divided into two main sections. In Section 2, we are reviewing briefly the fundamental considerations of the LIBS technique, and discussing the details of the experimental setup and materials. In section 3, the atomic spectra of alloying elements (Mg, Mn, Cr, Cu, and Zn) and molecular spectra (AlO) in Aluminum alloys will be presented and discussed. Lastly, we will conclude with some remarks based on what was presented earlier.

2. Materials and Methods

2.1. Fundamental considerations in LIBS

2.1.1. Plasma formation

LIBS is essentially based on the laser-matter interaction during the ablation of a small amount of material that is vaporized just after a laser pulse. If the power density is high enough [2] (~ 1GW/cm^2), atoms can absorb a photon from the laser beam and be ionized [18]. An ion is then formed as an electron is becoming free from a given atom. In the case of nanosecond pulses, the generation of heat will dominate the ionization process. Some more details on the heat process will be discussed in the next section. Free electrons from the ionization process can then oscillate with respect to ions and a plasma is being initiated. If an electron in the atom absorbs a photon from the laser beam or from another emitting atom, it can also transit from an upper quantum level to a lower level and emit a spectral line characterizing a given atomic element. As free electrons are not oscillating far from the ions, it can also be absorbed by an atom and emit under the recombination process. Signatures from small concentrations of alloying elements in a metal can be detected using the LIBS technique. In this report, we will also discuss the diatomic molecular emission of aluminum monoxide (AlO) and compare our results with the findings of other authors.

2.1.2. Generation of heat

LIBS investigations used nanoseconds [19,20], picoseconds [21] and femtoseconds [21,22] lasers in the near infrared, excimer in the UV [23] and CO_2 laser in the mid-infrared [24]. In the case of a femtosecond pulse with a duration of typically 100 fs interacting on metals, the energy is absorbed by free electrons, which thermalize and reach rapidly to a high temperature T_e. The electron cooling time is in the order of 1 ps and the lattice heating time is a few hundred ps [25]. This means that the heat transfer between the electron and the lattice can be neglected. Ionization in the case of a femtosecond pulse is a non-thermal effect and other processes such as tunneling, multi-photon absorption and avalanche ionization will dominate [26] in the initiation of the plasma. As the nanosecond pulse duration is longer than the electron-lattice heating time, heat is dominant in the ionizing process. Picosecond pulses can produce similar LIBS spectrogram as femtosecond pulses [21,27,28], but generate more heat for the same reason afore-mentioned. As very much attention was devoted to nanosecond pulse laser over the past decade, we will present data in section 4 for the LIBS method to detect small amount of alloying elements in Aluminum (Al 2024, Al 5086, Al 5456 and Al 7075). These four different types of Al with different material compositions are listed in Table 1 with details on the chemical contents of the alloying elements. These four types of Al were carefully selected to better discriminate traces of alloying elements from the spectral lines observed in all the spectrograms recorded. All spectrograms presented were verified to be reproducible with our experimental set-up.

2.1.3. Time delay between the nanosecond laser Q-switch and the spectrometer

A plasma is characterized by a transient nature in its early life. The typical life time is 10 μs and its dimensions are on the order of a few millimeters in full expansion. If the data are recorded too early, the intensity is very high and it is masked by strong radiation such as inverse Bremsstrahlung [29] and other radiation such as the attraction of a large number of electrons colliding with the positively charged target being investigated. At this stage, spectroscopic lines are difficult to detect within this strong radiation background. The plasma expands to reach its full dimension and starts cooling off. Recording spectra are desirable near the full expansion which is on the order of microseconds. In

 doi:10.20944/preprints202402.0890.v1

many laser-induced plasma investigations [8,30,31], the energy per pulse is within the 50-275 mJ range, the pulse duration is typically 5 to 20 ns and a delay within the 1-20 μs range is applied between the laser Q-switch and the start of the data acquisition. Parameters on pulse energy, pulse duration and time delay will be set within the aforementioned range for all the samples being investigated in this report.

2.2. Experimental Details

2.2.1. LIBS on detection of alloying elements

A Q2HE nanosecond laser delivering 100 mJ pulse with a duration of 5 ns emitting at λ=1053 nm was used in the investigation on Aluminum (Al) samples. All investigations in the Al samples were done at a repetition rate of 20 Hz. A time delay within 1μs and 5μs was set after the 5 ns pulse and then 20 shots of laser pulse were fired on each sample. All spectrograms show the average of the seven last laser shots. The computed standard deviation from the average of the last seven shots is typically 5% for all Al samples during our investigations. The lightweight spectrometer (175 g) used is an AvaSpec-Mini 4096CL with CMOS semiconductor. This handheld spectrometer can be used to set a delay of a microsecond or more between a Q-switch of a 5 ns pulse Q2HE laser from Quantum Light Instruments and the start of the data acquisition. A handheld spectrometer is used due to the easy integration in compact airborne systems such as a drone payload. The results presented will show that the performance of this handheld spectrometer is promising for rapid on-site inspection. Figure 1 shows LIBS experimental setup and a typical sample in a custom mounting piece.

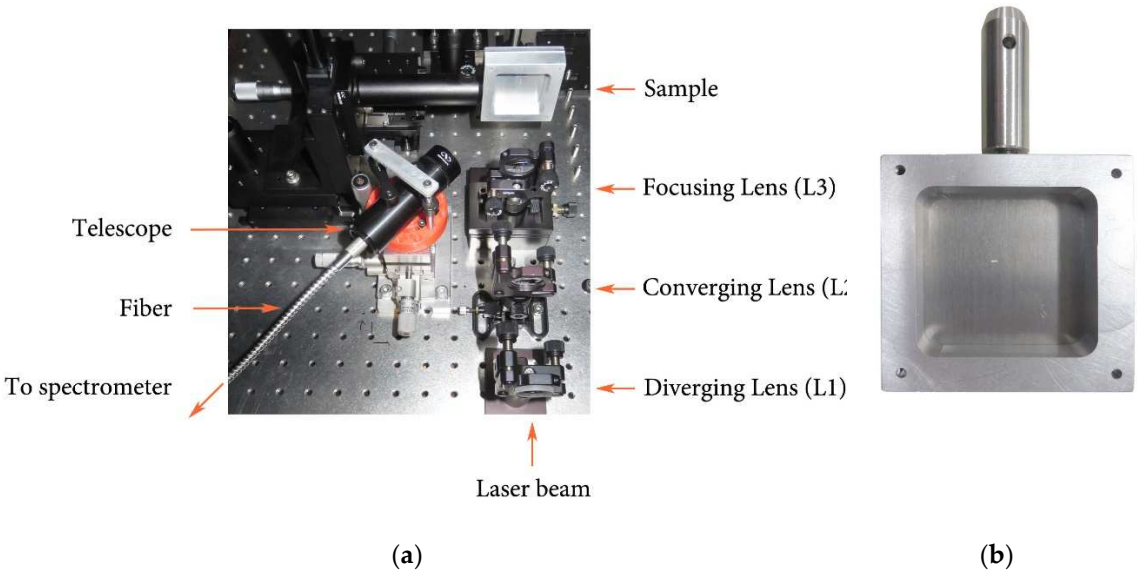

Figure 1. (**a**) LIBS Experimental setup; (**b**) Typical sample in its custom mounting piece.

2.2.2. Samples

The industrial aluminum alloy plates used in this study—Aluminum 5456 (Al 5456), Aluminum 5086 (Al 5086), Aluminum 7075 (Al 7075), and Aluminum 2024 (Al 2024)—were purchased from McMaster-Carr [32]. Al 5456 and Al 5086 are high-strength marine aluminum and are primarily used as a structural material for the construction of marine vessels. Al 7075 and Al 2024 are high-strength aluminum and are primarily used for aircraft structural components. Large Al alloy plates ranging in size from 15 cm x 15 cm to 30 cm x 30 cm were cut into smaller 5 cm x 5 cm plates suitable for our experimental setup. Measurements were carried out on several smaller plates to confirm the reproducibility of the results for each aluminum alloy.

These particular aluminum alloys were chosen for our study due to differences in their material composition. The amount of magnesium (Mg) in these four alloys ranges from 1.2 to 5.5%. The amount of zinc (Zn) in AL 7075 ranges from 5.1 to 6.1%, which significantly exceeds the Zn content

 doi:10.20944/preprints202402.0890.v1

in all other samples (less than 0.25%). The amount of copper (Cu) is significant in Al 7075 and Al 2024 (from 1.2 to 4.9%), while in the other two alloys it is present in much smaller quantities (less than 0.1%). Al 5456, Al 5086 and Al 7075 contain more Cr compared to AL 2024. The concentration of Manganese (Mn) is progressively increasing in all Al samples investigated. The material composition of the studied aluminum alloys is presented in Table 1.

Table 1. Material composition of aluminum alloys Al 7075, Al 5086, Al 5456, and Al 2024 according to the manufacturer [32].

Material	Material Composition (%)						
	Al	**Cr**	**Cu**	**Mg**	**Mn**	**Zn**	**Other**
AL 7075	87.1-91.42	0.18-0.287	1.2-2.0	2.1-2.9	0-0.3	5.1-6.1	0-0.15
AL 5086	93-95.7	0.05-0.25	0-0.1	3.5-4.5	0.2-0.7	0.25	0.15
AL 5456	91.8	0.05-0.2	0.1	4.7-5.5	0.5-1.0	0.25	0.2
AL 2024	90.75-94.7	0-0.1	3.8-4.9	1.2-1.8	0.3-0.9	0-0.25	0.015

3. Results and Discussion

3.1. Aluminum and alloying elements

Figure 2 shows each spectrogram for a given Al sample within three different spectral ranges with an appropriate scale to appreciate the performance of the LIBS technique in detecting the emission lines from various alloying elements. Note that the alloying elements have been identified using arrows. The experimental and documented spectral line wavelengths are also shown in Table 2.

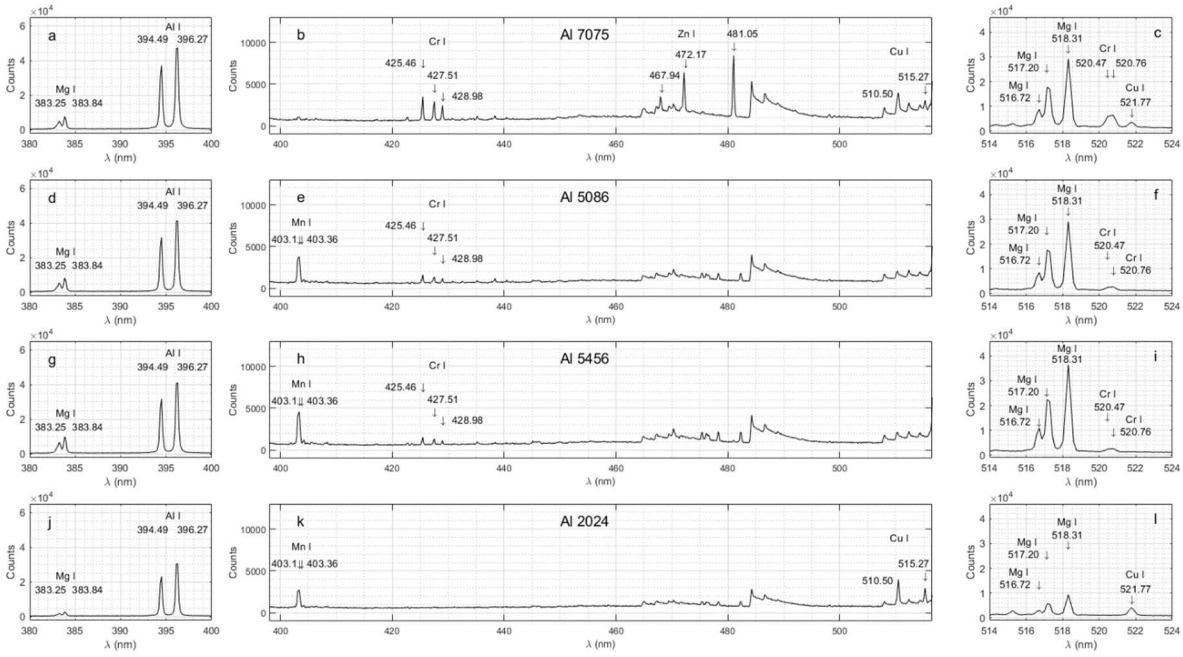

Figure 2. Al 7075 after a 5μs delay: (**a**) within 380-400 nm; (**b**) within 400-516 nm; (**c**) within 514-524 nm. Al 5086 after a 5μs delay: (**d**) within 380-400 nm; (**e**) within 400-516 nm; (**f**) within 514-524 nm. Al 5456 after a 5μs delay: (**g**) within 380-400 nm; (**h**) within 400-516 nm; (**i**) within 514-524nm. Al 2024 after a 5μs delay: (**j**) within 380-400 nm; (**k**) within 400-516 nm; (**l**) within 514-524 nm.

Table 2. Intensities of atomic emission lines in Al 7075, Al 5086, Al 5456, and Al 2024, measured with a time delay of 5 μs.

Element	Measured	Documented Wavelength	Counts			
			Al 7075	Al 5086	Al 5456	Al 2024

 doi:10.20944/preprints202402.0890.v1

	Wavelength (nm)	(nm)				
Al I	394.49	394.40	37076	31839	31791	23280
	396.27	396.15	46869	41250	40686.3	30512
Mg I	383.25	383.23	5182	5633	6821	1997
	383.84	383.83	7827	8404	10070	2955
	516.72	516.73	8833	8501	10902	3104
	517.20	517.27	17703	17592	22498	5674
	518.31	518.36	29259	29091	36551	9313
Mn I	403.10	403.08	1051	3470	4040	2538
	403.36	403.31	1087	3797	4561	2746
	475.37	475.40	1590	1875	2133	1350
	467.1	476.15	1499	1738	1966	1302
	476.25	476.24	1409	1692	1960	1253
	476.54	476.59	1388	1617	1833	1481
	478.28	478.34	1346	1813	2190	1584
	482.36	482.35	1063	1793	2116	1290
Zn I	467.94	468.01	3509	-	-	-
	472.17	472.22	6412	-	-	-
	481.05	481.05	8431	-	-	-
	636.20	636.23	1829	-	-	-
Cr I	426.46	425.43	3487	1621	1532	-
	427.51	427.48	2728	1376	1334	-
	428.98	428.97	2455	1197	1143	-
	520.47	520.45	5983	2545	2515	-
	520.76	520.60	6433	2735	2656	-
	540.92	540.98	2150	1438	1485	-
Cu I	510.50	510.55	3961	-	-	3963
	515.27	515.32	3076	-	-	2949
	521.77	521.82	3583	-	-	4167

3.2. Aluminum (Al)

The strongest documented Al emission lines in the investigated range (330 nm – 890 nm) are the lines at 394.40 nm and 396.15 nm [33]. We detected Al I emission peaks at 394.49 nm and 369.27 nm in all samples. Figure 3 shows emission spectra of Al in Al 7075, Al 5456, Al 2024, and Al 5086 measured with time delays of 3 μs and 5 μs.

 doi:10.20944/preprints202402.0890.v1

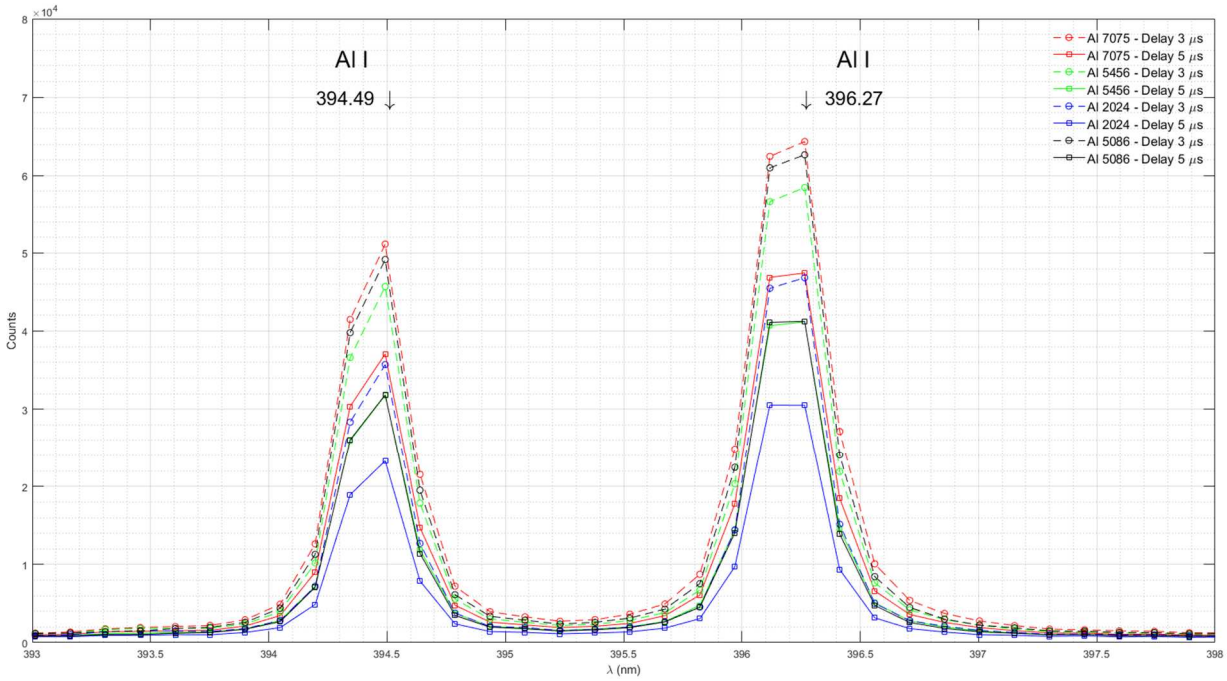

Figure 3. Emission spectra of Al in Al 7075, Al 5456, Al 2024, and Al 5086 measured with time delays of 3 μs and 5 μs.

The AvaSpec-Mini 4096CL spectrometer has a modest resolution of 0.09 nm. At this resolution, each Al I emission peak is defined by only two data points. The peak around 394.40 nm is defined by the measurements at 394.34 nm and 394.49 nm. The peak around 396.15 nm is defined by the measurements at 396.12 nm and 396.27 nm. The documented wavelengths for both Al I peaks lie between the measured data points. Therefore, it is likely that the actual peak intensity is greater than the measured intensity.

The Al content in the studied aluminum alloys ranges from 87.1% to 95.7%. Due to overlapping ranges for specific samples, the actual difference in aluminum concentration between samples may be as small as 1.5%. Our experimental results indicate that a higher resolution spectrometer would be useful for differentiating between samples with small differences in aluminum concentration based on Al I spectral lines.

All the measurements have been done for the time delays of 1 μs, 3 μs, and 5 μs. The measurements for the time delay of 5 μs have the best signal-to-noise ratio. As a result, the emission spectra in Figure 1 were shown for the time delay of 5 μs.

3.3. Magnesium (Mg)

Note that small amounts of alloying elements may also be detected. For example, magnesium (Mg) is present in all Al samples with varying chemical contents ranging from 1.2 to 5.5%. The strongest documented Mg emission lines in the investigated range (330 nm – 890 nm) are a doublet around 383.25 nm and 383.84 nm, and a triplet at 516.72 nm, 517.20 nm and 518.31 nm [33]. Other authors also identified these Mg emission lines [5]. Figure 4 shows emission spectra of Mg in Al 7075, Al 5456, Al 2024, and Al 5086 measured with time delays of 1 μs, 3 μs, and 5 μs.

 doi:10.20944/preprints202402.0890.v1

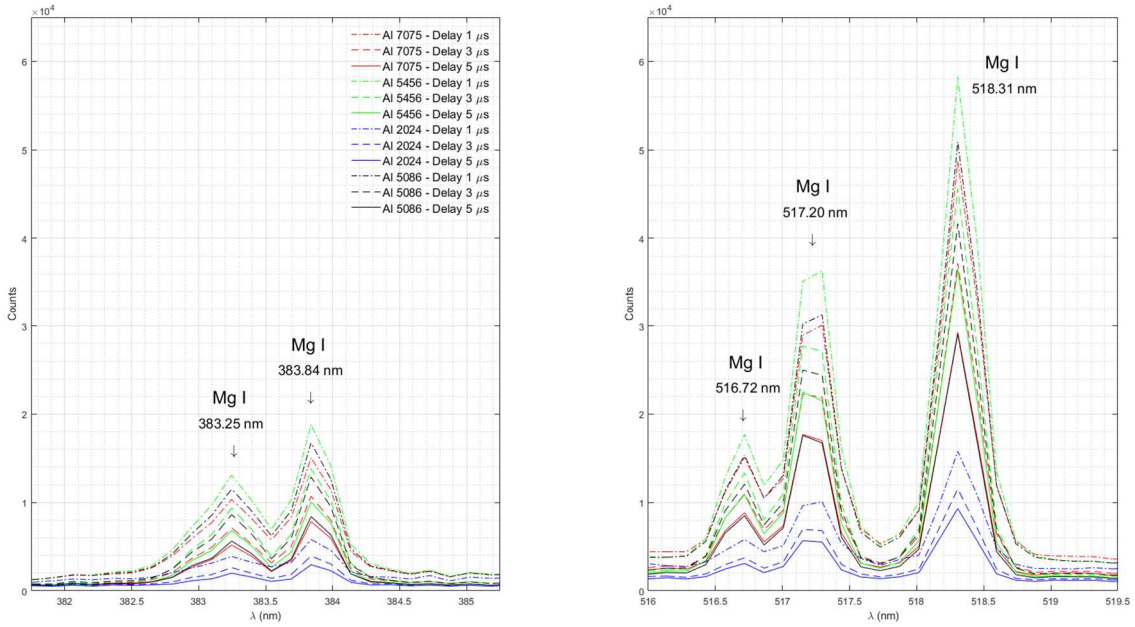

Figure 4. Emission spectra of Mg in Al 7075, Al 5456, Al 2024, and Al 5086 measured with time delays of 1 μs, 3 μs, and 5 μs.

The highest intensity of the emission line corresponds to Al 5456, the sample with the highest percentage of Mg (4.7-5.5%). The lowest intensity corresponds to Al 2024, the sample with the lowest amount of Mg (1.2-1.8%). The intensity of the Mg I emission lines for Al 5086 (3.5-4.5%) is slightly higher than for Al 7075 (2.1-2.9%), and both lie between the maximum (Al 5456) and minimum (Al 2024), as expected.

3.4. Manganese (Mn)

Figure 5 shows emission spectra of Mn in Al 7075, Al 5456, Al 2024, and Al 5086 measured with time delays of 3 μs and 5 μs.

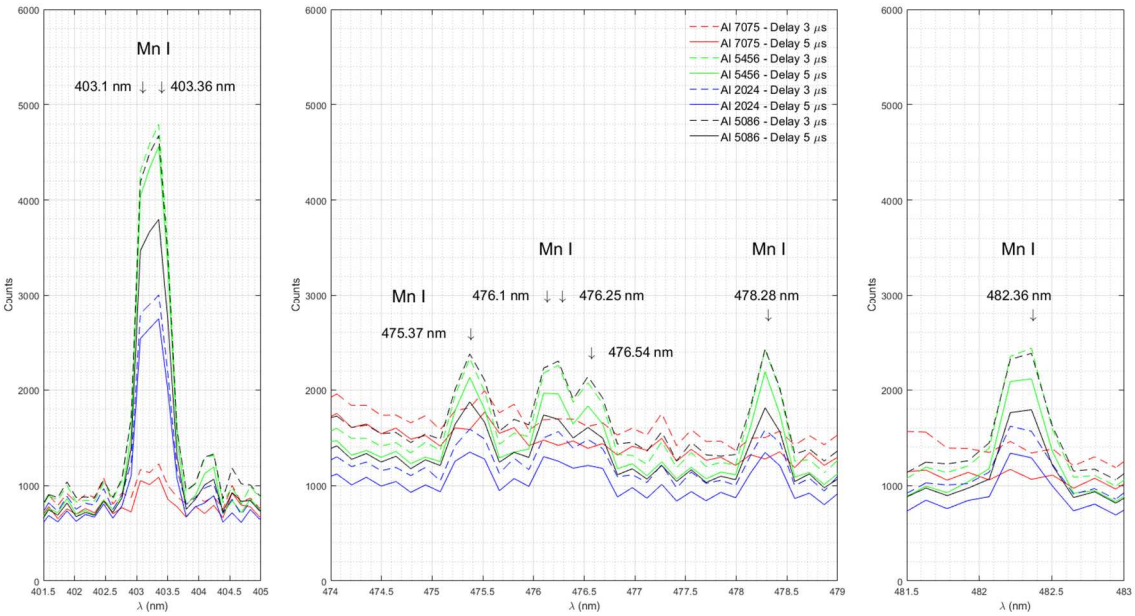

Figure 5. Emission spectra of Mn in Al 7075, Al 5456, Al 2024, and Al 5086 measured with time delays of 3 μs and 5 μs.

 doi:10.20944/preprints202402.0890.v1

The strongest documented Mn emission lines in the investigated range (330nm – 890 nm) are the lines at 403.08 nm and 403.31 nm [33]. Although the resolution of our spectrometer (0.09 nm) does not allow us to distinguish between these two lines of Mn doublet, we do see a broad line peaking between 403.06 to 403.36 nm in all samples. The highest intensity of the emission line corresponds to Al 5456, the sample with the highest percentage of Mn (0.5-1%). The lowest intensity corresponds to Al 7075, the sample with the lowest amount of Mn (0-0.3%). The intensity of the emission lines near 403 nm for Al 2024 (0.3-0.9 %) and Al 5086 (0.2-0.7) lies between the maximum (Al 5456) and the minimum (Al 7075) count values as expected. Our experimental results show that the LIBS method can determine a more precise measurement within a given range. Note that the intensity of the Mn I emission line at 403.36 nm for Al 5086 (count 3797) is greater than that of Al 2024 (count 2746). Although the chemical content ranges overlap for these two Al samples, it is possible to determine that Al 5086 is holding more Mn than Al 2024. We also observed emission lines of Mn near 475.37 nm, 476.1 nm, 476.25 nm, 476.54 nm, 478.28 nm, and 482.36 nm in our samples.

3.5. Zinc (Zn)

Figure 6 shows emission spectra of Zn in Al 7075 measured with time delays of 1 µs, 3 µs, and 5 µs.

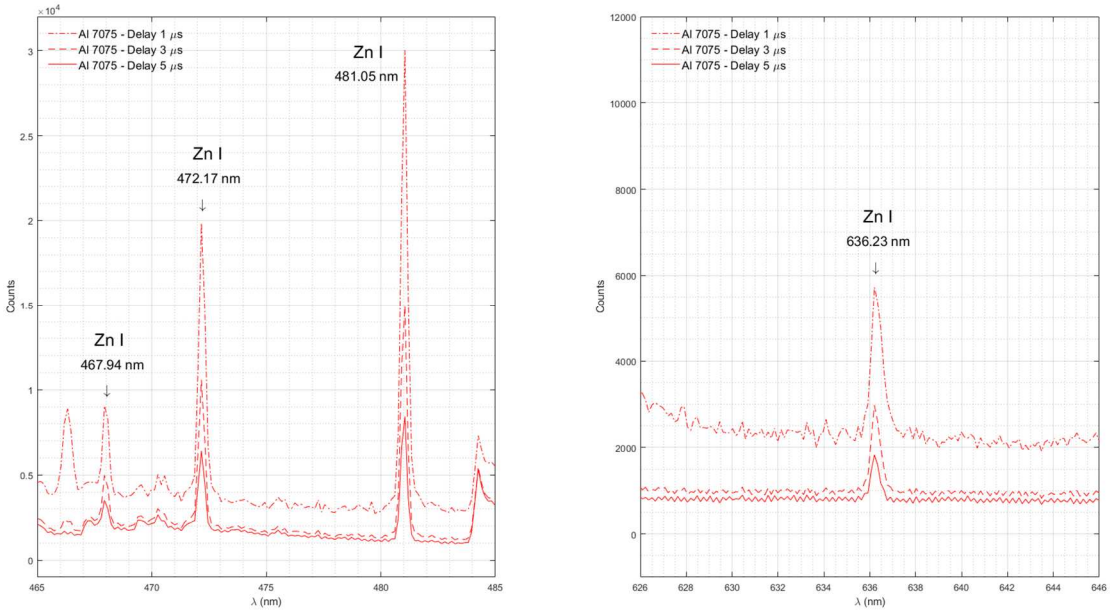

Figure 6. Emission spectra of Zn in Al 7075 measured with time delays of 1 µs, 3 µs, and 5 µs.

The strongest documented Zn emission lines in the investigated range (330 nm – 890 nm) are the lines at 468.01 nm, 472.22 nm, 481.05 nm, and 636.23 nm [33]. Our experimental data shows all Zn lines in Al 7075, which is the sample with the largest percentage of Zn (5.1-6.1%). Zn emission lines are absent in Al 5086 and Al 5456, both with a Zn content of about 0.25%, and in Al 2024 with the lowest Zn content (0-0.25%) among the studied samples. We did not observe Zn emission lines around 330.26 nm and 334.50 nm due to the poor quantum efficiency of our spectrometer [34].

3.6. Copper (Cu)

Figure 7 shows the emission spectra of Cu in Al 7075 and Al 2024 measured with time delays of 1 µs, 3 µs, and 5 µs.

 doi:10.20944/preprints202402.0890.v1

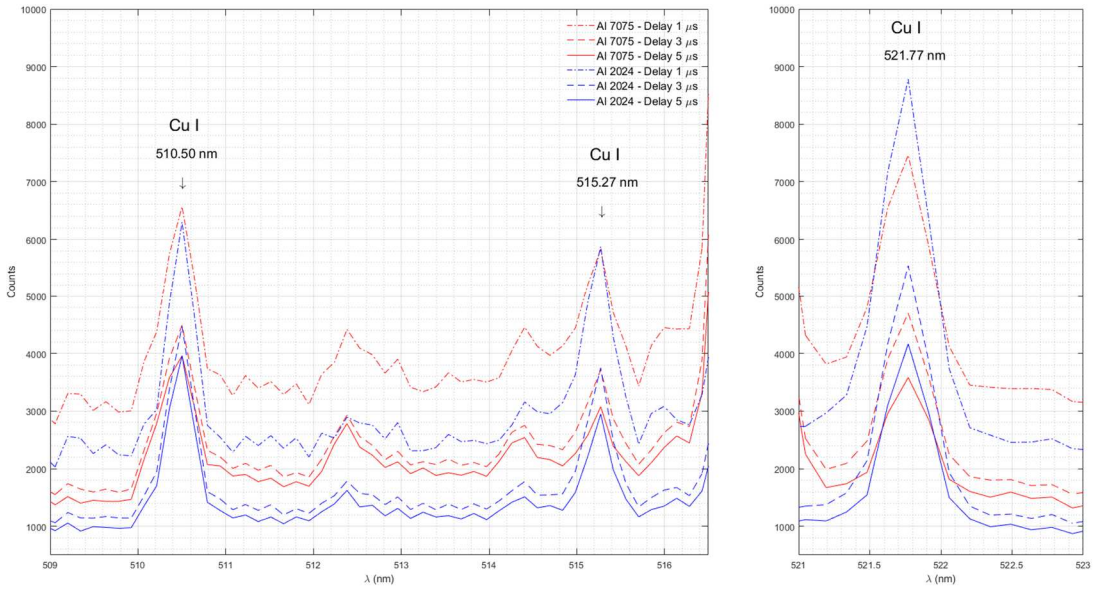

Figure 7. Emission spectra of Cu in Al 7075 and Al 2024 measured with time delays of 1 μs, 3 μs, and 5 μs.

The strongest documented Cu I emission lines in the investigated range (330 nm – 890 nm) are the lines at 510.55 nm, 515.32 nm, 521.82 nm, 324.75 nm, and 327.4 [33]. Other authors also identified these Cu emission lines [35]. Our experimental data shows Cu I emission lines with distinct peaks at 510.5, 515.27 and 521.77 nm in Al 2024, the sample with the highest amount of Cu (3.8-4.9%), as well as in Al 7075 , the sample with the second highest amount of Cu (1.2-2.0%). Cu I emission lines are absent in the spectra of Al 5086 and Al 5456, both with the lowest Cu content (0–0.1%). We did not observe Cu emission lines near 324.75 nm and 327.4 nm due to the poor quantum efficiency of our spectrometer [34].

3.7. Chromium (Cr)

Figure 8 shows the emission spectra of Cr in Al 7075, Al 5456 and Al 5086 measured with time delays of 1 μs, 3 μs, and 5 μs.

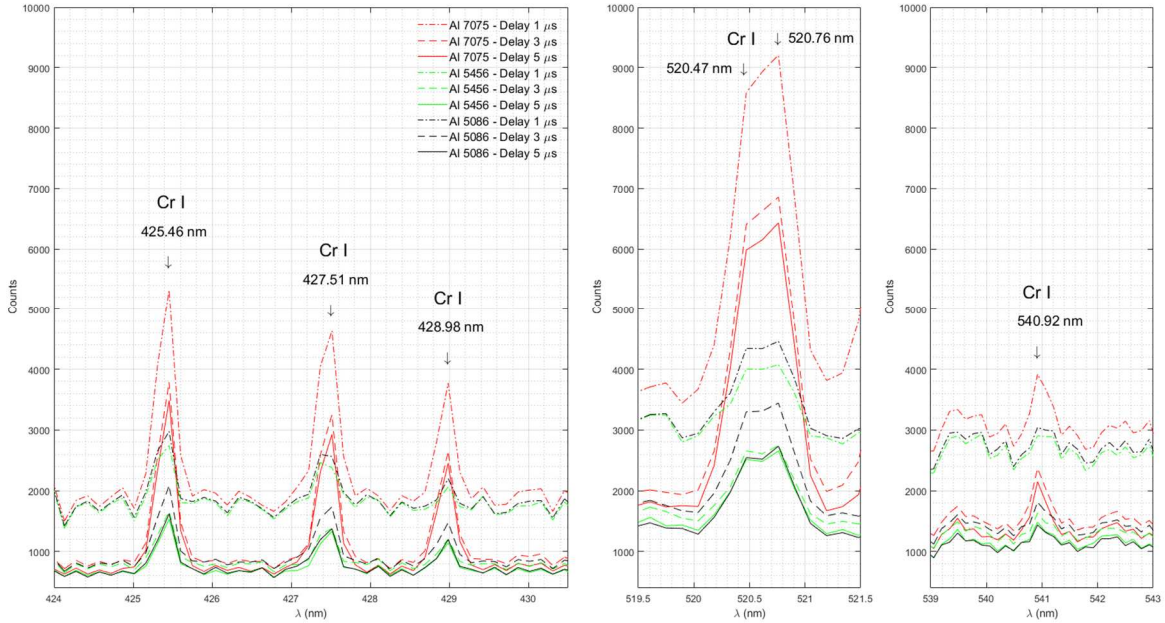

Figure 8. Emission spectra of Cr in Al 7075, Al 5456 and Al 5086 measured with time delays of 1 μs, 3 μs, and 5 μs.

 doi:10.20944/preprints202402.0890.v1

The strongest documented Cr I emission lines in the investigated range (330 nm – 890 nm) are the lines at 425.43 nm, 427.48 nm, 428.97 nm, 520.45 nm, 520.60 nm, and 540.98 nm [33]. Our experimental data show a Cr I triplet with well-defined peaks at 426.46, 427.51 and 428.98 nm, a broad line with a maximum between 520.47 and 520.76 nm and a well-defined peak at 540.92 nm in Al 7075 , the sample with the largest amount of Cr (0.18-0.287%), as well as in Al 5086 (0.05-0.25% Cr) and Al 5456 (0.05-0.2% Cr). Cr I emission lines are absent in Al 2024 with the lowest Cr content (0-0.1%).

3.8. Aluminum Monoxide (AlO)

Figure 9 shows emission spectra of AlO measured in Al 5456 with time delay 5 μs. Table 3 shows the intensities of the AlO diatomic emission spectra for the bands Δν= +1, Δν= 0, Δν= -1 and Δν= -2, measured in Al 5456 with a time delay of 5 μs.

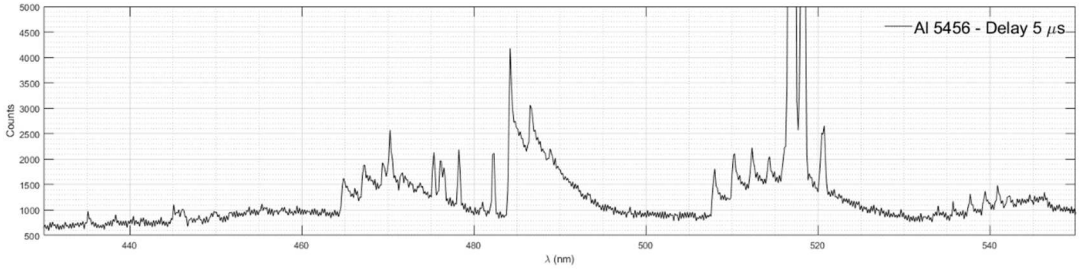

Figure 9. Diatomic emission spectra of AlO measured in Al 5456 with time delay 5 μs.

Table 3. Intensities of AlO diatomic spectra for Δν = +1, Δν = 0, Δν = -1 and Δν = -2 bands, measured in Al 5456 with a time delay of 5 μs.

AlO molecular transitions	Measured Wavelength (nm)	Estimated Wavelength (nm) [36]	Counts (Al 5456)
Δν= +1	464.87	465.0	1623
	467.21	467.0	1877
	469.4	469.3	1927
	471.73	471.0	1733
	473.77	473.3	1537
Δν= 0	484.25	484.3	4178
	486.58	486.6	3062
	488.9	488.8	2204
Δν= -1	508.04	507.8	1807
	510.36	510.0	2108
	512.38	512.1	2223
	514.41	514.2	2049
Δν= -2	534.02	533.3	1082
	535.74	535.3	1172
	537.76	537.3	1314
	539.48	539.1	1366
	540.92	540.8	1485
	542.36	542.1	1277

The molecular emission of AlO after laser-induced optical breakdown was studied in detail by C.G. Parigger [36–38]. Other authors also identified presence of AlO in aluminum alloys centered at 466.4 nm without time delay. In this investigation no rotational activity of diatomic molecular was identified in the spectra [39]. Our experimental results in this report are consistent with the findings

 doi:10.20944/preprints202402.0890.v1

of C.G. Parigger et al. Each rotational wavelength for AlO was computed based on theoretical model for the Δv = 0, ±1, ±2 and +3 bands by C.G. Parigger and J.O. Hornkohl [36,37]. We compared our experimental data for the Δv = +1, 0, -1, -2 bands with the theoretical predictions of these authors. The estimated wavelength values of the peaks are shown in the Table 3.

3.8.1 Δv = 0 band

Peaks near 484.25 nm, 486.58 nm, and 488.9 nm can be attributed to the Δv= 0 band.

3.8.2. Δv=+1. band

The emission spectra of atoms and molecules are superimposed in the spectral region of the band Δv = +1. Peaks near 464.87 nm, 467.21 nm, 469.4 nm, 471.73 nm and 473.77 nm can be attributed to the Δv = +1 band. The peak near 470.27 nm can be attributed to the atomic emission of Cr I. Peaks near 475.37 nm, 476.1 nm, 476.25 nm, 476.54 nm, 478.28 nm, and 482.36 nm can be attributed to the atomic emission of Mn I, as shown in Figure 5.

3.8.3. Δv=-1. band

The emission spectra of atoms and molecules are superimposed in the spectral region of the band Δv = -1. Peaks near 508.04 nm, 510.36 nm, 512.38 nm, and 514.41 nm can be attributed to the Δv = -1 band. The triplet near 516.72 nm, 517.2 nm, and 518.31 nm corresponds to the atomic emission spectra of Mg I, as shown in Figure 4. A broad line with the maximum between 520.47 and 520.76 nm corresponds to the atomic emission spectra of Cr I, as shown in Figure 8.

3.8.4. Δv=-2. band

Peaks near 534.02 nm, 535.74 nm, 537.76 nm, 539.48 nm, 540.92 nm, and 542.36 nm can be attributed to the Δv = -2 band. The line around 540.92 nm also corresponds to the atomic emission spectrum of Cr I, as shown in Figure 8.

5. Conclusions

It was shown that a handheld spectrometer with a modest spectral resolution can identify various alloying elements in Aluminum. Some molecular activity of AlO can also be identified as long as an adequate time-delay is used, which may be depending on the kinetic time of the oxide formation. The rotational and vibrational spectra of the AlO molecule are comparing very well with the experimental and theoretical works of other authors [36–38]. In future work, the same results can be obtained on a high resolution spectrometer to obtain more precision on the linewidth by obtaining more data points on each line. This would allow one to compute the electron density from the linewidth. A spectrometer with a better resolution can also identify emissions from certain ions that are ionized twice under the same conditions, and temperature of the plasma can then be determined from Saha-Boltzmann plots.

Author Contributions: Conceptualization, Luc Lévesque; Data curation, Svetlana Rytchkova and Luc Lévesque; Formal analysis, Svetlana Rytchkova and Luc Lévesque; Funding acquisition, Luc Lévesque; Investigation, Svetlana Rytchkova and Luc Lévesque; Methodology, Svetlana Rytchkova; Project administration, Svetlana Rytchkova and Luc Lévesque; Resources, Luc Lévesque; Software, Luc Lévesque; Supervision, Luc Lévesque; Validation, Svetlana Rytchkova and Luc Lévesque; Visualization, Svetlana Rytchkova; Writing – original draft, Svetlana Rytchkova; Writing – review & editing, Svetlana Rytchkova and Luc Lévesque.

Funding: This research was funded by the Directorate Technical Airworthiness and Engineering Support (DTAES 8, Canada, Grant number 18485S7104).

Institutional Review Board Statement: Not applicable

Informed Consent Statement: Not applicable

Data Availability Statement: All relevant data used in this manuscript can be accessed through the corresponding author.

Conflicts of Interest: The authors declare no conflicts of interest.

References

1. Sankhla, M. S.; Kumari, M.; Nandan, M.; Kumar, R.; Agrawal, P. Heavy Metal Contamination in Water and their Hazardous Effect on Human Health-A Review. *Int. J. Curr. Microbiol. App. Sci* **2016**, *5(10)*, 759-766, doi: 10.20546/ijcmas.2016.510.082.
2. Senesi, G.S.; Dell'Aglio, M.; Gaudiuso, R. Heavy Metal Concentrations in Soils as Determined by LIBS, with Special Emphasis on chromium. *Environmental Research* **2009**, *109*, 413-420, doi: 10.1016/j.envres.2009.02.005.
3. Kim, G.; Kwak, J.; Kim, K. R.; Lee, H.; Kim, K. W.; Yang, H.; Park, K. Rapid Detection of Soils Contaminated with Heavy Metals and Oils by Laser Induced Breakdown Spectroscopy. *Journal of Hazardous Materials* **2013,** *263*, 754– 760, doi: 10.1016/j.jhazmat.2013.10.041.
4. Sezer, B.; Bilge, G.; Boyaci, I. H. Capabilities and Limitations of LIBS in Food Analysis. *Trends in Analytical Chemistry* **2017**, *97*, 345-353, doi: 10.1016/j.trac.2017.10.003.
5. Zhang, Y.; Zhao, Z.; Xu, T.; Niu, G.; Liu, Y.; Duan, Y. Characterization of local thermodynamic equilibrium in a laser-induced aluminum alloy plasma. *Appl. Opt.* **2016**, *55(10)*, 2741-2747, doi: 10.1364/AO.55.002741.
6. Alvarez**,** J.; Pacheco, P.; Sarmiento, R. Spectral and electrical characterization of an Aluminum plasma laser between the flat plates of a capacitor. *J. Phys: Conf. Ser.* **2019**, *1219*, 012009:1-012009:7, doi: 1742-6596/1219/1/012009.
7. Geertsen, C.; Lacour, J.L.; Mauchien, P.; Pierrard, L. Evaluation of laser ablation optical emission spectrometry for microanalysis in aluminum samples. *Spectrochim Acta Part B At Spectrosc* **1996**, *51*, 1403-1416, doi: 10.1016/0584-8547(96)01494-2.
8. Harilal, S.S.; Bindhu, C.V.; Isaac, R.C.; Nampoori, V.P.N.; Vallabhan, C.P.G. Electron density and temperature measurements in a laser produced carbon plasma. *J. Appl. Physics* **1997**, *82 (5)*, 2140-2146, doi: 10.1063/1.366276.
9. Ji, G.; Ye, P.; Shi, Y.; Yuan, L.; Chen, X.; Yuan, M.; Zhu, D.; Chen, X.; Hu, X.; Jiang, J. Laser-Induced Breakdown Spectroscopy for Rapid Discrimination of Heavy-Metal-Contaminated Seafood Tegillarca granosa. *Sensors* **2017**, *17(11)*, 2655, doi: 10.3390/s17112655.
10. Hedwig, R.; Lahna, K.; Lie, Z. S.; Parded, M.; Kurnanian, K. H.; Tjia, M. O.; Kagawa, K. Application of picosecond laser-breakdown spectroscopy to quantitative analysis of boron in meatballs and other biological samples. *Appl. Opt.* **2016,** *55(32)*, 8986-8992, doi: 10.1364/AO.55.008986.
11. Shahedi, A.; Eslami, E.; Nourani, M.R. Influence of Lead on the Interpretation of Bone Samples with Laser-Induced Breakdown Spectroscopy. JSPEC **2016,** *2016*, 8205479:1-8205479:6, doi: 10.1155/2016/8205479.
12. Samek, O.; Beddows, D.C.S.; Telle, H.H.; Morris, G.W.; Liska, M.; Kaiser, J. Quantitative analysis of trace metal accumulation in teeth using laser-induced breakdown spectroscopy. *Applied Physics A* **1999**, *69[Suppl.]*, S179-S182, doi: 10.1007/s003390051379.
13. Kumar, A.; Yueh, F.-Y.; Singh, J. P.; Burgess, S. Characterization of malignant tissue cells by laser-induced breakdown spectroscopy. *Appl. Opt.* **2004**, *43*, 5399–5403, doi: 10.1364/AO.43.005399.
14. Martin, M. Z.; Labbé, N.; André, N. High resolution applications of laser-induced breakdown spectroscopy for environmental and forensic applications. *Spectrochim Acta Part B At Spectrosc* **2007**, *62(12)*, 1426–1432, doi: 10.1016/j.sab.2007.10.046.
15. Giakoumaki, A.; Melessanaki, K.; Anglos, D. Laser-induced breakdown spectroscopy (LIBS) in archaeological science-applications and prospects. Anal. Bioanal. Chem. **2007,** *387*, 749-760, doi:10.1007/s00216-006-0908-1.
16. **Kaszewska, E.A.**; Sylwestrzak, M.; Marczak, J.; Skrzeczanowski, W.; Iwanicka, M.; Szmit-Naud, E.; Anglos, D.; Targowski, P. Depth-Resolved Multilayer Pigment Identification in Paintings: Combined Use of Laser-Induced Breakdown Spectroscopy (LIBS) and Optical Coherence Tomography (OCT). *Appl. Spectrosc.* **2013**, *67*, 960–972, doi: 10.1366/12-06703.
17. Noll, R.; Bette, H.; Brysch, A.; Kraushaar, M.; Mönch, I.; Peter, L.; Sturm, V. Laser-induced breakdown spectroscopy – Applications for production control and quality assurance in the steel industry. *Spectrochim Acta Part B At Spectrosc* **2001**, *56*(6), 637-649, doi: 10.1016/S0584-8547(01)00214-2.
18. Colao, F.; Lazic, V.; Fantoni, R.; Pershin, S. A comparaison of single and double pulse laser-induced breakdown spectroscopy of aluminum samples. *Spectrochim Acta Part B At Spectrosc* **2002**, *57*, 1167-1179, doi: 10.1016/S0584-8547(02)00058-7.
19. Harilal, S.S.; Issac, R.C.; Bindhu, C.V.; Varier, G.K., Nampoori, V.P.N.; Vallabhan, C.P.G. Spatial and time-resolved analysis of CN bands in the laser-induced plasma front graphite. *Pramana* **1996**, 46(2), 145-151, doi: 10.1007/BF02848230.
20. Shah, S.K.H.; Iqbal, J.; Ahmad, P.; Khandaker, M.U.; Haq, S.; Naeem, M. Laser induced breakdown spectroscopy method and applications: A comparative review. *Radiat. Phys. Chem.* **2020**, *170*, 108666:1-108666:23, doi: 10.1016/j.radphyschem.2019.108666.

21. Rohwetter, P.; Yu, J.; Méjean, G.; Stelmaszczyk, K.; Salmon, E.; Kasparian, J.; Wolf, J.-P.; Wöste, L. Remote LIBS with ultrashort pulses: characteristics in picosecond and femtosecond regimes. *J. Anal. At. Spectrom.* **2004**, *19*, 437-444, doi: 10.1039/B316343A.
22. Labutin, T.A.; Lednev, V.N.; Ilyin, A.A.; Popov, A.M. Femtosecond laser-induced breakdown spectroscopy. *J. Anal. At. Spectom.* **2016**, *31*, 90-118, doi: 10.1039/c5ja00301f.
23. De Giacomo, A. Experimental characterization of metallic titanium-laser induced plasma by time and space resolved optical emission spectroscopy. *Spectrochim Acta Part B At Spectrosc* **2003**, *58(1)*, 71-83, doi: 10.1016/S0584-8547(02)00234-3.
24. Lehmann, S.; Fischer, M.; Rosin, A.; Gerdes, T.; Krenkel, W. The feasibility of CO_2-laser-induced breakdown spectroscopy for fast lead determination in glass cullet. *Int. J. Appl. Glas. Sci.* **2020**, *11*, 369-379, doi: 10.1111/ijag.14653.
25. Momma, C.; Nolte, S.; Chichkov, B.N.; Alvensleben, F.V.; Tünnermann, A. Precise laser ablation with ultrashort pulses. *Applied Surface Science* **1997**, *109/110*, 15-19, doi: 10.1016/S0169-4332(96)00613-7.
26. Anabitarte, F.; Cobo, A.; Lopez-Higuera, J. M. Laser-Induced Breakdown Spectroscopy: Fundamentals, Applications, and Challenges. *ISRN Spectroscopy* **2012**, *2012*, 285240:1-285240:12, doi:10.5402/2012/285240.
27. Le Drogoff, B.; Margot, J.; Chakar M. et al., Temporal characterization of femtosecond laser pulses induced plasma for spectrochemical analysis of aluminum alloys. *Spectrochim Acta Part B At Spectrosc* **2001**, *56(6)*, 987-1002, doi: 10.1016/S0584-8547(01)00187-2.
28. *Laser-Induced Breakdown Spectroscopy*, 1st ed.; Singh, J.P., Thakur, S.N., Eds.; Elsevier: Amsterdam, The Netherlands, 2007; ISBN 978-0-444-51734-0, doi: 10.1016/B978-0-444-51734-0.X5001-7.
29. Dutouquet, C. LIBS Detection of Nanomaterials for Process Control and in the Workplace. *Spectroscopy* **2015**, *30(4)*, 24-33, doi: ineris-01852967.
30. Elhassan, A.; Abd Elmoniem, H.M.; Kassem, A.K.; Hairth, M.A. Effect of applying static electric field on the physical parameters and dynamics of laser-induced plasma. *J. Adv. Res.* **2010,** *1(2)*, 129-136, doi: 10.1016/j.jare.2010.03.004.
31. Alvarez, J.; Pacheco, P.; Sarmiento, R. Spectral and electrical characterization of an aluminum plasma between the flat plates of a capacitor. *J. Phys.: Conf. Ser.* **2019**, *1219*(1), 12009, doi: 10.1088/1742-6596/1219/1/012009.
32. McMaster-Carr. Available online: https://www.mcmaster.com/ (accessed on 13 February 2024).
33. National Institute of Standards and Technologies. Atomic Spectra Database (2021). Available online: https://physics.nist.gov/asd (accessed on 13 February 2024).
34. Lee, J. S.; Hornsey, R.I.; Renshaw, D. Analysis of CMOS Photodiodes – Part I: Quantum Efficiency. *IEEE Transaction on electron devices* **2003**, *50(5)*, 1233-1238, doi: 10.1109/TED.2003.813232.
35. Kurniawan, G.; Sa'adah, F.; Khumaeni, A. Emission characteristics of copper using laser-induced breakdown spectroscopy at low pressure. *J. Phys.: Conf. Ser.* **2018**, *1025*, 012003:1-012003:5, doi: 10.1088/1742-6596/1025/1/012003.
36. Parigger, C.G. Atomic and molecular emissions in laser-induced breakdown spectroscopy. *Spectrochim Acta Part B At Spectrosc* **2013**, *79-80*, 4-16, doi: 10.1016/j.sab.2012.11.012.
37. Parigger, C.G.; Hornkohl, J.O. Computation of AlO $B^2\Sigma^+ \rightarrow X^2\Sigma^+$ emission spectra. *Spectrochim Acta Part A* **2011**, *81(1)*, 404-411, doi: 10.1016/j.saa.2011.06.029.
38. Parigger, C. G.; Woods, A. C.; Witte, M. J.; Swafford, L. D.; Surmick, D. M. Measurement and analysis of atomic hydrogen and diatomic molecular AlO, C2, CN, and TiO spectra following laser-induced optical breakdown. *J. Vis. Exp.* **2014,** *84*, 51250:1–51250:8, doi: 10.3791/51250.
39. Lévesque, L.; Woodcock, K.; Prezgot, D. Laser-induced emission spectra of stainless steels and aluminum irradiated with nanopulse lasers without setting delay: potential applications to remote sensing and laser micromachining. *Appl. Opt.* **2022**, *61(27)*, 7937-7947, doi: 10.1364/AO.462496.